# (Non)Equilibrium of OH and Differential Transport in MILD Combustion

Najafi, S. B. Nourani; van Oijen, J. A.; Levinsky, H. B.; Mokhov, A.

*Published in:*
Energy & fuels

*DOI:*
10.1021/acs.energyfuels.1c00583



*Publication date:*
2021

energy&fuels

pubs.acs.org/EF

Article

# (Non)Equilibrium of OH and Differential Transport in MILD Combustion: Measured and Computed OH Fractions in a Laminar Methane/Nitrogen Jet in Hot Coflow

S. B. Nourani Najafi, J. A. van Oijen, H. B. Levinsky, and A. V. Mokhov*

Cite This: *Energy Fuels* 2021, 35, 6798–6806

Read Online

ACCESS | Metrics & More | Article Recommendations

**ABSTRACT:** Spatial distributions of temperature, major species, and OH mole fractions under moderate or intense low-oxygen-dilution (MILD) conditions in a laminar-jet-in-hot-coflow configuration were measured using spontaneous Raman and laser-induced-fluorescence methods. A preheated mixture of 18% $CH_4$/82% $N_2$ at 1100 K was used as fuel, while the products of a laminar, flat, premixed burner-stabilized flame with an equivalence ratio of 0.8 at 1550 K were used as the oxidizer. For comparison, experiments replacing the fuel by pure $N_2$ were also performed. The measurements are compared with the results of numerical simulations performed using the GRI-Mech 3.0 chemical mechanism and a multicomponent mixture-averaged transport model. Analysis of the data shows that the maximum axial and radial temperature and OH mole fraction occur on the lean side of the stoichiometric mixture fraction. MILD combustion generates maximum OH mole fractions of ∼700 ppm in the radial profiles close to the burner exit and ∼300 ppm along the centerline, more than five times lower than those measured in equivalent methane/air diffusion flames. Overall, good qualitative and quantitative agreement is found between the results of detailed computations and experiments, with the maximum differences observed in the axial OH profiles, which are just outside the estimated experimental uncertainty. Analysis of the computational results shows that differential diffusion hinders the use of the mixture fraction to estimate the equilibrium temperature and species fractions, causing an overestimation of the stoichiometric temperature by ∼200 K. Calculating the equilibrium quantities based on the local (computed) species fractions shows an axial temperature profile that differs from that experimentally/computationally determined by less than 25 K. The analysis further shows that the measured OH mole fractions are roughly three times higher than the (locally determined) equilibrium value.

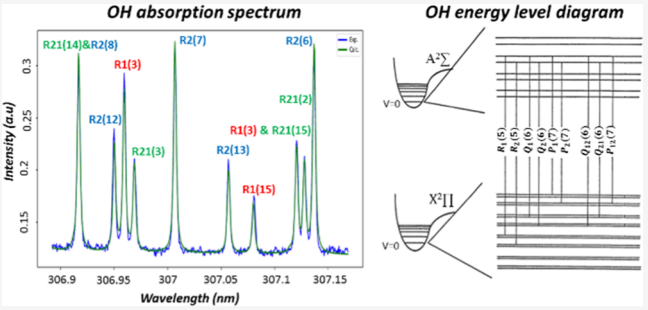




## 1. INTRODUCTION

The desire to limit global warming and reduce the emissions of pollutants such as $NO_x$ is driving innovation in clean and efficient energy-utilization technology in high-temperature industrial processes. Moderate or intense low-oxygen-dilution (MILD) combustion, also called flameless combustion, is a method to achieve high thermal efficiency, with concomitant fuel savings and $CO_2$ reduction, while maintaining low pollutant emissions.[1] This technique applies highly preheated and diluted air and/or fuel to obtain a homogeneous temperature distribution with low $NO_x$ formation. The process is characterized[1,2] by the relatively low temperature increase during combustion. Despite its increasing use in industry, more fundamental understanding of the microscopic physical and chemical processes is needed to facilitate the effective application of MILD combustion to the wide variety of industrial processes and fuels.[1−4]

Several experimental and numerical studies in a turbulent jet in hot coflow (JHC) under MILD conditions have been performed to provide insights into the structure of the reaction zone. In particular, Dally et al.[2,5] experimentally investigated the effect of oxygen concentration in a turbulent hot coflow in a hydrogen−methane flame under MILD conditions. Their results showed that reducing the oxygen mass fraction from 9 to 3% in the hot oxidant stream results in considerable changes in the flame structure. These changes include a strong decrease in peak temperature, of up to 400 K, and a threefold decrease in OH and CO fractions, which suggested different chemical pathways under different conditions. Salavati-Zadeh et al.[3] numerically studied the experimental conditions of Dally et al.[2] to investigate the effect of molecular diffusion in the turbulent

Received: February 22, 2021
Revised: March 12, 2021
Published: March 26, 2021

JHC under MILD conditions. They observed a noticeable improvement in the prediction of the OH mass fractions near the fuel inlet plane by considering the molecular diffusion with a proper Schmidt number for each species.

Although MILD combustion is most often applied under turbulent conditions in high-temperature furnaces, understanding the spatial structure observed under laminar conditions[6] is required for modeling of large-scale MILD combustion. Laminar coflow diffusion flames have been a standard object for the investigation of salient details of nonpremixed combustion systems to provide insights into the chemical structure of flames. Comprehensive experimental and computational studies of structures of these flames have been performed.[7−9] More recently,[6,10−12] the distribution of major species, temperature, and NO have been studied under laminar MILD conditions, both experimentally and numerically, in a laminar-jet-in-hot-coflow (LJHC) configuration. In refs 6 11, and 12, it was shown that a two-dimensional (2-D) computational model with detailed chemistry could faithfully predict the measured species in this system. However, under these relatively low-temperature conditions, the question arises regarding the degree of nonequilibrium of the radical species in these flames. Under the high-temperature and oxygen-rich conditions extant in many flames, chain-branching reactions (such as $H + O_2 = OH + O$) are much faster than the radical-recombination reactions that dominate the approach to equilibrium,[13,14] resulting in substantial nonequilibrium radical fractions in the flame and postflame zones. However, to our knowledge, it is yet to be determined what the effects are of the relatively low temperatures and low oxygen fraction in MILD combustion on the size of the radical pool.

The hydroxyl radical is one of the key reactive species in the oxidation of hydrocarbon fuels. The importance of OH, combined with the fact that its local concentration can be quantified straightforwardly using laser-induced fluorescence (LIF), makes it a good candidate to assess the degree of (non)equilibrium in MILD combustion systems. To date, there have been few experimental and numerical studies of the OH fraction in laminar MILD flames. Arndt et al.[15] investigated the autoignition of a pulsed methane jet issuing into a laminar coflow of hot exhaust products of a lean premixed hydrogen/air flat flame using OH planar laser-induced fluorescence (PLIF), OH* chemiluminescence, and broadband flame luminosity measurements. The study from the PLIF images showed that autoignition tended to occur at the interface between "bulges" of the inflowing jet and the coflow and, for steady-state conditions, autoignition was observed frequently below the flame base. Evans et al.[16] studied laminar MILD flames of natural gas and $C_2H_4$ in a JHC burner using high-speed images to establish a distinction between the MILD and normal combustion regimes. Their results showed that the OH* chemiluminescence becomes more intense when the oxygen content in the hot coflow is increased.

To our knowledge, the literature describing combined experimental and computational determination of the OH mole fraction in laminar coflow flames under MILD conditions is lacking. In the present study, the spatial distribution of the OH mole fraction in MILD combustion in an LJHC geometry is determined by LIF, under conditions reported in previous studies.[6,10−12] The local gas temperature and the fractions of major species, needed to extract the OH mole fraction from the LIF signal, are obtained from measurements using spontaneous Raman scattering. The measured spatial profiles are compared with the predictions of the two-dimensional laminar axisymmetric numerical simulations reported earlier.[6,11]

## 2. EXPERIMENTAL SETUP

The LJHC burner is the same as that used in ref 10 and is shown schematically in Figure 1 and described briefly here. The flows and

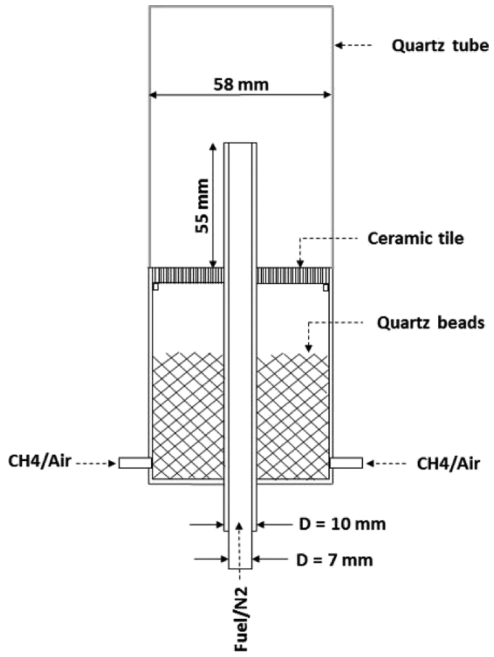


**Figure 1.** Schematic of the LJHC burner.

compositions used here are exactly the same as those that gave MILD combustion in ref 10. For the coflow, a hot oxidizer stream is formed by the combustion products of a flat $CH_4$/air premixed flame stabilized on a ceramic plate with the equivalence ratio $\varphi = 0.8$ and an average exit velocity of 15.5 cm/s (under standard conditions). The velocity profile in the coflow is homogenized by glass beads. A quartz tube is used to improve the stability of the flame and to prevent mixing of the oxidizer with ambient air. In the inner tube, either a mixture with composition 18% $CH_4$/82% $N_2$ or pure nitrogen at an average exit velocity of 5.8 cm/s (at standard conditions) is used to supply fuel to the combustion zone. The compositions and temperatures of the resultant hot flows in the measurement/computational domain are given in Table 1. The gas flows are

**Table 1. Inlet Composition (Mole Fractions) and Temperature of Fuel and Oxidizer Streams of MILD Flame**

| oxidizer | | | | | fuel | | |
|---|---|---|---|---|---|---|---|
| $[O_2]$ | $[N_2]$ | $[CO_2]$ | $[H_2O]$ | $T$ (K) | $[N_2]$ | $[CH_4]$ | $T$ (K) |
| 0.036 | 0.732 | 0.087 | 0.145 | 1550 | 0.82 | 0.18 | 1100 |

measured using calibrated Bronkhorst mass flow meters. The burner is moved axially and radially by a positioner (Parker) with positioning uncertainty less than 0.1 mm.

The local gas temperature and mole fractions of major species ($CO_2$, $H_2O$, $N_2$, $CH_4$, $O_2$, CO, and $H_2$) were measured using spontaneous Raman scattering, while the OH mole fractions were obtained by LIF. The schematic of the experimental setup is shown in Figure 2. The optical scheme for the spontaneous Raman measurements is essentially identical to that described in ref 17. In the present study, 40 pixels of the CCD camera along the laser beam are binned,


https://doi.org/10.1021/acs.energyfuels.1c00583
Energy Fuels 2021, 35, 6798−6806

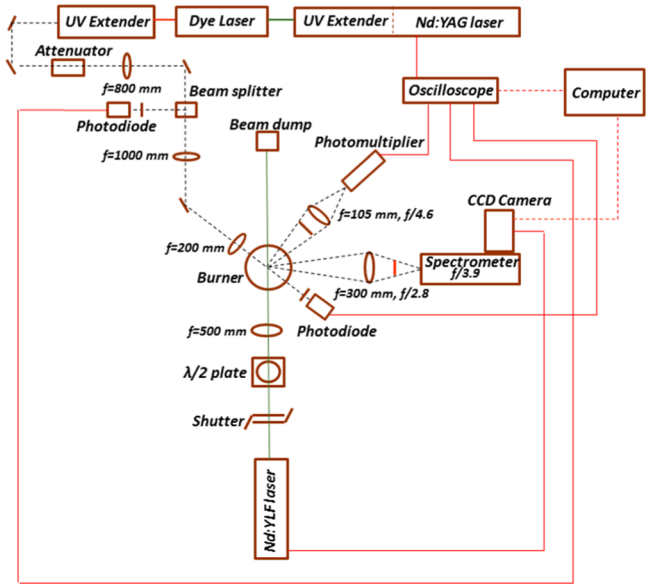


**Figure 2.** Schematic of the experimental setup.

integrating the signal over a distance of roughly 1 mm, yielding the spatial resolution of the temperature and major species mole fraction measurements in the horizontal direction. The vertical resolution is estimated to be of the same order. The temperature measurements are performed using $N_2$ Raman spectra recorded at moderate resolution (about 0.1 nm), while the mole fraction measurements of main flame species are carried out at lower resolution (about 1 nm). The performance of the Raman setup is tested by comparing measurements in premixed flames stabilized above a McKenna burner at various equivalence ratios with the equilibrium calculations. In this regard, the gas flow rates are set sufficiently high to create "free" flames where adiabatic temperatures and equilibrium concentrations of main components are expected. Based on these comparisons, we estimate the accuracy of the temperature measurements to be better than 2% and the accuracy of the Raman fractions to be better than 10% for flame species with mole fractions ≥0.05.

For the LIF measurements, a Sirah PrecisionScan tunable dye laser with a UV extender is pumped by a Spectra-Physics Quantra Ray Pro 250-10 Nd:YAG laser and is scanned in the vicinity of the $R_2(7)$ OH rotational line near 306.8 nm in the $A^2\sum \rightarrow X^2\prod(0-0)$ vibrational band. To assure linearity of the LIF signal, which was verified experimentally, the laser pulse energy is decreased to 20 $\mu J$ by an attenuator. The power of the laser beam before and after passing through the burner is measured by Newport UV-enhanced silicon PIN photodiodes. The laser beam is focused into the center of the burner by a quartz lens ($f$ = 200 mm), providing the spatial resolution ∼1 mm perpendicular to the laser beam. Fluorescence is collected at a right angle by a Nikkor camera quartz lens ($f$/4.5, $f$ = 105 mm) and detected by an Electron Tubes 9659QB photomultiplier. A bandpass filter with a center wavelength of 306 nm and a bandwidth of 8 nm is used to select the fluorescence from (0−0) vibrational bands of the $A^2\sum \rightarrow X^2\prod(0-0)$ electronic band. A pinhole installed in front of the photomultiplier yields a spatial resolution along the laser beam of ∼1 mm. The signals from the photodiodes and the photomultiplier are digitized by a 600 MHz oscilloscope (Agilent 54830B) and stored in a computer for further processing. The laser is tuned in a spectral range of 0.0125 nm with the step 0.0005 nm in the vicinity of the $R_2(7)$ OH rotational line. One hundred laser pulses are averaged for every point in the scan, which results in a total measurement time of ∼4 min for a single OH LIF excitation spectrum. To avoid excessive measurement times associated with quantifying the entire computational domain, only the axial profile and radial profiles at heights 3, 12, and 25 mm above the exit of the fuel tube are measured, similar to that carried out previously.[6,10,11] We remark here that the distributions of measured temperatures and major species mole fractions were within the experimental uncertainty of those reported earlier.[6,10]

The LIF OH measurements are performed in the linear regime, where the LIF signal integrated over the absorption line can be presented as[18]

$$I_{FL} = \frac{C^*S_{line}{}^*E_L{}^*X_{OH}}{T^*Q(T)^*Z(T)} \quad (1)$$

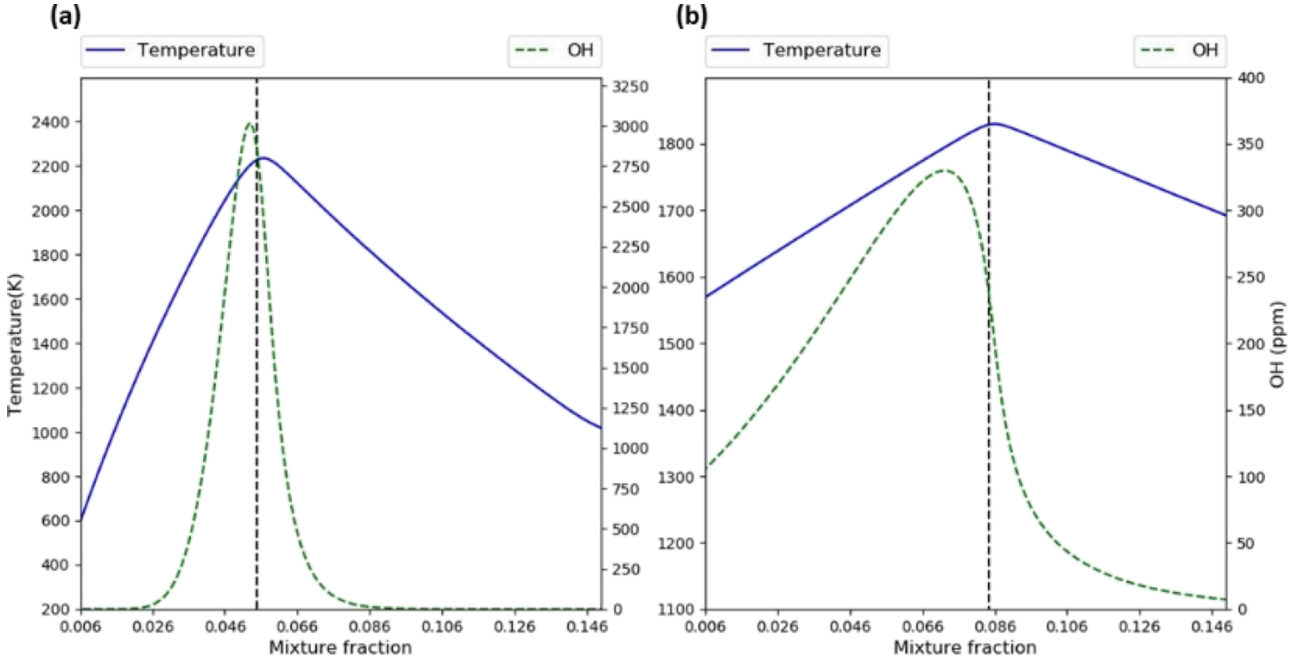


**Figure 3.** Equilibrium temperature and OH mole fraction vs mixture fraction in the methane/air diffusion flame using reactants at room temperature (a) and the "MILD flame" using the conditions given in Table 1 (b). The vertical dashed lines mark the stoichiometric mixture fraction.


https://doi.org/10.1021/acs.energyfuels.1c00583
Energy Fuels 2021, 35, 6798−6806

Here, $I_{FL}$ is the integrated fluorescence intensity obtained by scanning the laser wavelength in the vicinity of the vibrational−rotational absorption line, $E_L$ is the laser pulse energy, $Q(T)$ is the collisional deactivation (quenching) rate, $Z(T)$ is the partition function, $S_{line}$ is the spectral line strength, $X_{OH}$ is the OH mole fraction, and C is the proportionality constant depending upon parameters of the experimental setup. The spectral line parameters are taken from ref 19, and the quenching rates were calculated using quenching cross sections reported in ref 20 and the measured temperature and the major species fractions. To determine the absolute value of the OH mole fraction, multipoint calibration was performed by measuring OH fluorescence intensity at a height of 10 mm above the McKenna burner in premixed, burner-stabilized $CH_4$/air flames. The OH mole fraction was varied using different equivalence ratios ($\varphi$ = 0.8 and 1.0) and by varying the degree of stabilization (and thus the actual flame temperature) by varying the mass flux of the fuel/air mixture through the burner. The OH mole fractions and temperatures of the reference flames were also measured by direct absorption in premixed flames and compared with calculations using the PREMIX code in the CHEMKIN package[21] with the GRI-Mech 3.0[22] chemical mechanism. The observed variation in the LIF signal, corrected for temperature and quenching with the computed/measured OH fraction, was linear as expected from eq 1. The agreement between the measured and calculated OH mole fraction is roughly 30% which is taken here as the accuracy of the OH measurements.

## 3. RESULTS AND DISCUSSION

To facilitate the analysis below, we recall the convenience of describing the structure of a diffusion flame using the mixture fraction ($\xi$). To aid in the discussion, we compare the equilibrium temperature and OH mole fraction calculated using the inlet conditions in Table 1 with those for a diffusion flame using undiluted, room-temperature methane and air ("methane/air flame"). Both the equilibrium temperature and OH mole fraction for the methane/air diffusion flame (Figure 3a) are seen to be much higher than those for the MILD flame (Figure 3b); the temperature for the diffusion flame is 400 K higher and the OH fraction is roughly nine times higher than those under the MILD condition. We also note that the maximum equilibrium OH fraction in the diffusion flame is roughly a factor of 2 lower than that which has been measured under these conditions.[7]

**3.1. Structure of the MILD Flame.** To illustrate the overall MILD flame structure and anticipate the comparisons below, we consider the computed false color images of the distributions of temperature and OH mole fraction shown in Figure 4a,b, respectively. The computations used for comparison with measurements of the LJHC flame presented here were taken from refs 6 and 11. Described in detail in ref 6, the computational method solves the governing equations using the GRI-Mech 3.0. Transport is described by a mixture-averaged model in which the diffusion velocity of each species is calculated by assuming Fickian diffusion. In the conservation of energy, radiative heat loss is neglected. We note that similar to the comparisons reported in ref 11, the fuel composition in the measurements is 5% different than those in the computations (18 vs 17% methane), which aside from this modest difference agreed to within the measurement uncertainty. The mixture fraction has been calculated from species mole fractions using Bilger's formula,[23] modified to account for the presence of C and H in the oxidizer for the MILD case which is presented as

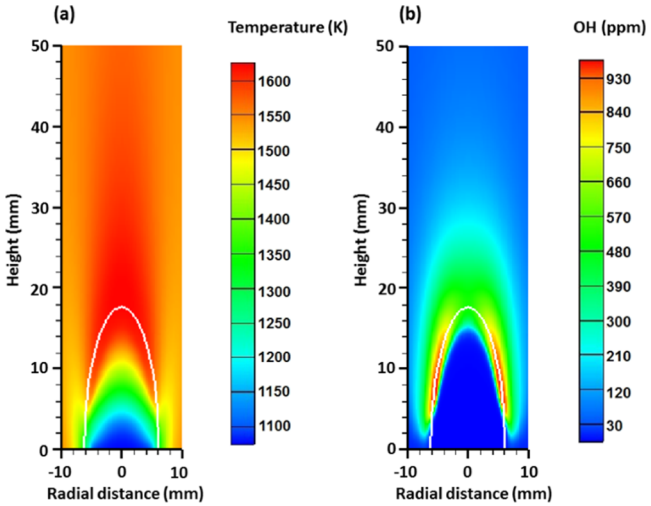


**Figure 4.** False color images of the temperature and OH mole fraction in the MILD flame. The white solid lines indicate the stoichiometric surface.

$$\xi \equiv \frac{\frac{2(Z_{C,2}-Z_C)}{W_C}+\frac{0.5(Z_{H,2}-Z_H)}{W_H}+\frac{Z_{O,2}-Z_O}{W_O}}{\frac{2(Z_{C,2}-Z_{C,1})}{W_C}+\frac{0.5(Z_{H,2}-Z_{H,1})}{W_H}+\frac{Z_{O,2}}{W_O}} \quad (2)$$

where $Z_j$ and $W_j$ are the elemental mass fractions and atomic masses for the elements C, H, and O, and the subscripts 1 and 2 refer to values in the fuel and coflow streams. The vertical zero ($z$ = 0) in the images corresponds to the fuel tube exit. As can be seen, both calculated distributions show the typical conical shape of Bunsen-type diffusion flames[24] where the combustion occurs around a "wishbone-shaped" stoichiometric surface ($\xi = \xi^{st}$), indicated by the white lines in Figure 4. The stoichiometric mixture fraction crosses the centerline at $z$ = 17 mm and crosses the exit plane of the fuel tube at the radial distance $r \sim 6$ mm, just outside the outer wall of the fuel tube (at $r$ = 5 mm).

Following the development of the temperature field from the fuel inlet, the temperature first increases and reaches a maximum of ∼1600 K and then slightly decreases. As can be seen, the maximum flame temperature occurs at positions almost coinciding with those of the stoichiometric mixture fraction. In the lean region, the temperature gradients relax substantially but are still present at $z$ = 50 mm. It should be pointed out that the maximum temperature in Figure 4 is ∼200 K lower than the stoichiometric "MILD flame" temperature (see Figure 3b), suggesting that combustion products are not in equilibrium around the stoichiometric mixture fraction.

In contrast to the appearance of the temperature distribution, the OH mole fraction has a qualitative resemblance to the wishbone form of a pure diffusion flame:[8] a relatively narrow spatial distribution, with larger gradients in the radial direction than along the centerline ($r$ = 0). Thin regions of OH embedded in a uniform temperature field were observed for MILD conditions in a turbulent jet in hot coflow.[25] Following the distribution downstream from the fuel inlet, the OH mole fraction first increases to ∼900 ppm around the stoichiometric surface, which is substantially higher than that at the inlet of the hot coflow (∼100 ppm). Further downstream, the OH mole fraction decreases as a result of recombination and dilution with the oxidizer. While the


https://doi.org/10.1021/acs.energyfuels.1c00583
Energy Fuels 2021, 35, 6798−6806

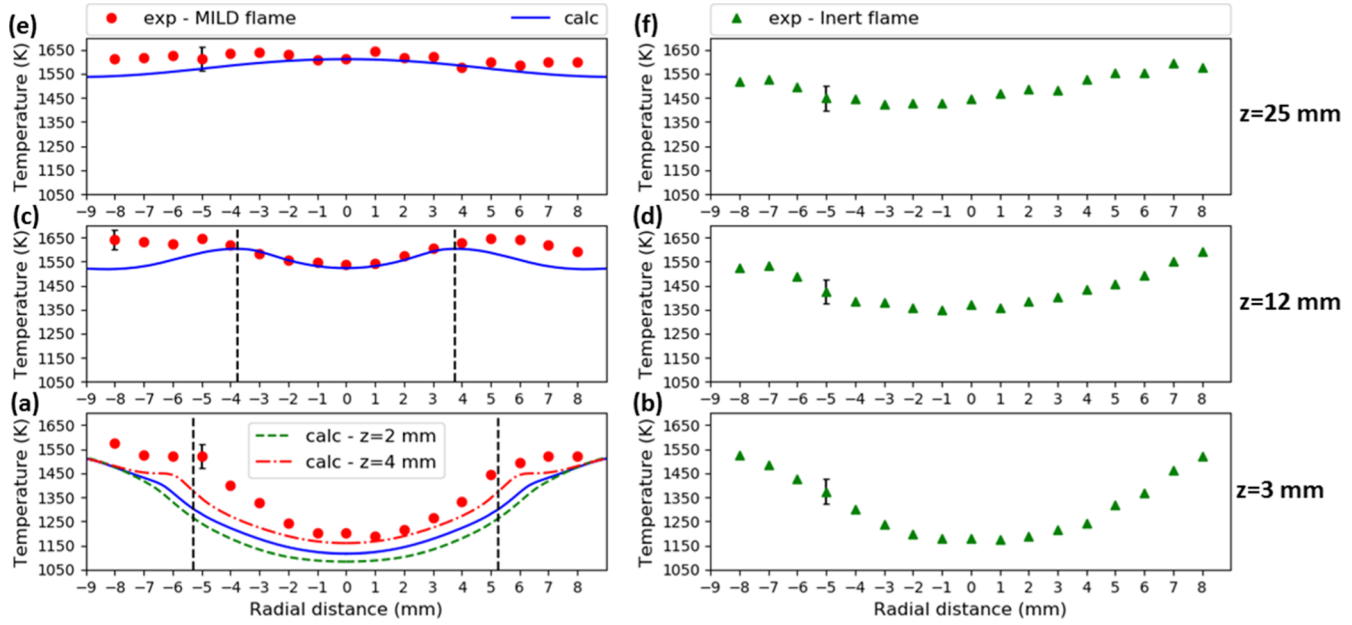


**Figure 5.** Radial profiles of temperature in MILD (left column) and "inert" (right column) flames at different heights. The vertical dashed lines mark the position of the stoichiometric mixture fraction.

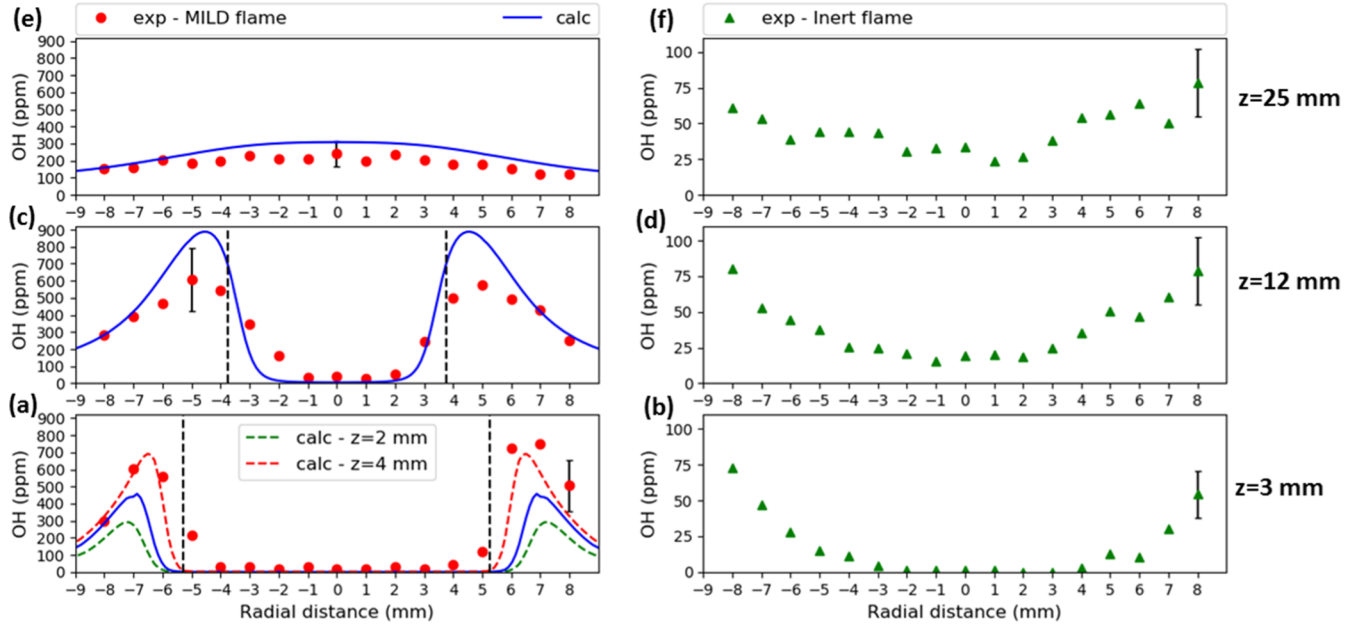


**Figure 6.** Radial profiles of the OH mole fraction in MILD (left column) and "inert" (right column) flames at different heights. The vertical dashed lines mark the position of the stoichiometric mixture fraction.

maximum calculated flame temperature in Figure 4a is ∼200 K lower than the maximum equilibrium temperature (Figure 3b), the maximum calculated OH mole fraction is nearly three times higher than equilibrium. For comparison with a non-MILD flame, the maximum calculated OH mole fraction is three times lower than the equilibrium stoichiometric "methane/air flame" OH mole fraction in Figure 3a. Similar to that observed in typical diffusion flames,[8] the maximum OH fraction on the centerline is significantly lower, by almost a factor of 2, than that in the radial maxima. We also note that the maximum temperatures and OH mole fractions computed for the MILD LJHC are similar to those reported for turbulent MILD conditions.[2]

**3.2. Radial Profiles of Temperature and the OH Mole Fraction.** The measured and computed radial temperature profiles at $z$ = 3, 12, and 25 mm above the fuel tube exit for the MILD flame are shown in Figure 5e, respectively. For comparison, the temperature profiles obtained with pure $N_2$ in the fuel tube inlet (denoted as the "inert flame") are also shown on the right side (Figure 5b,d,f), as carried out previously.[10] At $z$ = 3 mm, the radial temperature distribution increases from ∼1150 K at the centerline to ∼1550 K in the hot coflow. While temperatures close to the centerline for the two cases at this height, shown in Figure 5a,b, are the same within the experimental uncertainty, inspection of the MILD flame at this height shows small shoulders in both the


https://doi.org/10.1021/acs.energyfuels.1c00583
Energy Fuels 2021, 35, 6798−6806

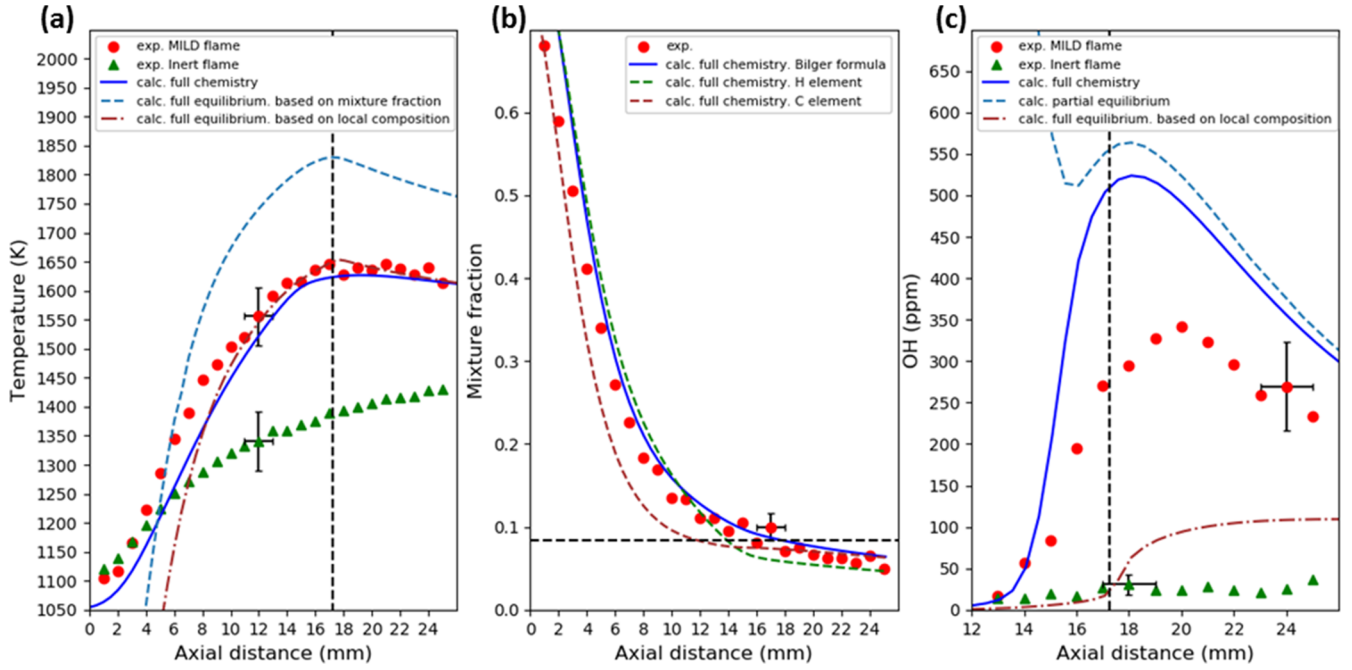


**Figure 7.** Axial profiles of the temperature (a), mixture fraction (b), and OH mole fraction (c). The dashed lines mark the position of the stoichiometric mixture fraction.

measured and the calculated temperature profiles at radial distances ($r$) between 5 and 7 mm from the centerline, which indicate the locations of the heat release around the stoichiometric surface.[6] At $z$ = 12 mm, the difference between the MILD and "inert" flames becomes more visible (Figure 5c,d), with the temperature at the centerline increasing to ∼1550 K. At this axial position, chemical reactions have increased the centerline temperature by ∼200 K as compared to the "inert flame". At $z$ = 25 mm, the temperature distribution of the MILD flame is almost uniform (Figure 5e), while the temperature distribution of the "inert flame" still shows a (slight) minimum around $z$ = 0.

A comparison between the measured and the calculated temperature profiles in the MILD flame shows an overall good agreement; the maximum discrepancy (∼100 K) is observed at $z$ = 3 mm. We ascribe this difference to the spatial resolution of the optical setup and the uncertainty in determining the vertical position of the measuring volume, which were estimated to be ∼1 mm in the present study. Figure 5a also shows the calculated temperature profiles at $z$ = 2 and 4 mm: a downstream shift of the calculations by 1 mm substantially improves the agreement.

The measured and calculated radial profiles of the OH mole fraction at $z$ = 3, 12, and 25 mm are shown for the MILD flame in Figure 6e, respectively. For comparison, the OH profiles at the corresponding axial distances measured in the "inert flame" are also shown in Figure 6b,d,f. While in the "inert flame" at $z$ = 3 mm (Figure 6b), the OH mole fraction monotonically increases with radial position from 0 at the centerline to ∼100 ppm in the hot coflow, relatively sharp peaks are observed at the same height at $r$ ∼ 7 mm in the MILD flame (Figure 6a), with their maximum slightly to the lean side of the stoichiometric mixture fraction, as reported in methane/air diffusion flames.[8] The sharpness of the OH profiles in Figure 6a,c, as compared to the temperature profiles in Figure 5a,c, allows tracking the slow progression of the radial position of the stoichiometric surface toward the centerline with increasing axial distance; the maximum at $z$ = 3 mm (Figure 6a) moves from $r$ ∼ 7 to ∼5 mm at $z$ = 12 mm above the burner (Figure 6c). It is interesting to note that while at this height, the centerline temperature of the MILD flame is ∼200 K higher than that of the "inert flame" and the OH mole fraction at the centerline is still very low. Clearly, at the extant temperature, consumption of OH by the fuel on the rich side of the stoichiometric surface prevents diffusion to the centerline.[8] Further downstream, at $z$ = 25 mm, the OH distribution of the MILD flame is almost uniform (Figure 6e), while the OH distribution of the "inert flame", being governed by diffusion and recombination, like the corresponding temperature profile still shows a minimum around the centerline. We observe that the maximum measured OH mole fractions (∼700 ppm) are more than a factor of 5 lower than those measured in (diluted) methane/air diffusion flames.[7,8]

Comparison of the measured and calculated OH profiles in the MILD flame indicates some differences at $z$ = 3 and 12 mm. The calculated OH mole fraction profiles have slightly sharper peaks than those in the measured profiles, which is at least partially attributable to the spatial resolution of the optical setup and uncertainty in the vertical position of the measuring volume. As for the radial temperature profile shown in Figure 5a, comparing the measured OH profile at $z$ = 3 mm with the computed profile at $z$ = 4 mm (Figure 6a) gives significantly better agreement in form and magnitude of the OH mole fraction. We further observe that the peaks in the radial OH profiles are somewhat broader than those observed in laminar diffusion flames,[7,8] similar to the observation for the width of the radial peaks in temperature made previously.[6,10]

**3.3. Axial Profiles.** The axial profiles of temperature, mixture fraction, and OH mole fraction along the centerline of the MILD and "inert" flames are shown in Figure 7. The centerline temperature (Figure 7a) in the MILD flame increases from ∼1100 K at the fuel tube exit to the maximum value ∼1650 K around $z$ = 17 mm and remains almost uniform


https://doi.org/10.1021/acs.energyfuels.1c00583
Energy Fuels 2021, 35, 6798−6806

at larger axial distances. As discussed above, the measured temperature difference between the MILD flame and the "inert flame" is less than 20 K at $z$ = 4 mm and then increases to ∼200 K at $z$ = 25 mm (Figure 7a). For both the temperature and mixture fraction calculated using modified Bilger's formula (Figure 7b), the computed results for the MILD flame match the experiments well. Shifting the profiles by 1 mm brings the profiles into near-quantitative agreement, consistent with the improvement observed in the radial profiles noted above. The maximum temperature is observed around the stoichiometric mixture fraction near $z$ = 17 mm (indicated by the horizontal line in Figure 7b), as expected.

Turning to the axial OH profiles in Figure 7c, we note that at $z$ < 13 mm, the OH mole fraction at the centerline is below the detectability limit of the present optical experimental setup and is not shown in the figure. In the MILD flame, the OH fraction increases further downstream to a maximum of ∼350 ppm at roughly $z$ = 20 mm and then decreases to ∼250 ppm at $z$ = 25 mm. As discussed regarding Figure 6a,c, the maximum in the OH mole fraction lies on the lean side of stoichiometry. Despite its low fraction as compared to methane/air diffusion flames,[7,8] the OH profile clearly indicates activity in the MILD radical pool when in contrast with the OH mole fractions measured in the "inert flame", also shown in Figure 7c. In the "inert flame", the centerline OH fraction does not exceed 30 ppm, which itself is lower than the ∼75 ppm in the oxidizer inlet shown in Figure 6, above. Comparing the computed OH fractions with the measurements in Figure 7c, we see that while the profiles are qualitatively similar, the maximum computed OH fraction is ∼50% larger than the measured maximum, (just) outside the estimated uncertainty in the measurement. This discrepancy cannot be attributed to either the spatial resolution of the present optical experimental setup or a 1 mm shift in profiles because of a relatively small spatial gradient in the axial direction. Differences between measured OH fractions in turbulent MILD flames and those computed using GRI-Mech 3.0 in one-dimensional (1-D) counterflow have also been observed previously;[5] there they allowed for the possibility that the kinetics determining the OH fraction may require improvement for MILD conditions.

With an eye toward mechanism reduction for facilitating numerical simulations, such as for turbulent flames, we also compare the "full-chemistry" calculations and experimental results with those calculated by assuming various degrees of equilibrium. Initially, the equilibrium calculations have been carried out using the compositions and enthalpies of the input streams as a function of the mixture fraction. The equilibrium temperatures at the mixture fractions corresponding to those calculated by the modified Bilger's formula at the same axial position are shown in Figure 7a (dashed line). As can be seen, the equilibrium temperature computed by this method shows the ∼200 K temperature difference at the stoichiometric mixture fraction with both measurements and "full-chemistry" computations, as discussed in the following Figure 4, above, and observed previously.[10] Given this large temperature difference, the question arises as to the possible contribution of any nonequilibrium OH and other radicals to this discrepancy. We first note that the equilibrium OH fraction along the centerline computed from the compositions and enthalpies of the input streams (not shown) is actually very close to the measurements given in Figure 7c; however, this OH fraction belongs to a much higher temperature and is thus clearly inappropriate for comparison with the measurements. Second, we consider the OH mole fraction based on partial equilibrium in the $H_2/O_2$ system.[7,26] To do so, we calculate the OH fractions using the relation $[OH] = (K_1K_2[H_2][O_2])^{1/2}$, where $K_1$ and $K_2$ are equilibrium constants for fast two-body reactions H + $O_2$ = OH + O and O + $H_2$ = OH + H, respectively. Since the computed major species are generally within 10% of the measurements[6,10] and recalling that the $H_2$ and $O_2$ fractions are low in the experiments, we use the computed species profiles for this purpose. The results are included in Figure 7c (dashed line) and show that the partial equilibrium assumption is within 10% of the detailed simulations from the stoichiometric mixture fraction to the end of the computational domain. It is thus reasonable to assume partial equilibrium among the radicals in the MILD flame under lean conditions, despite the relatively low temperature.

To quantify the contribution of radical nonequilibrium to the flame temperature, we performed the following computational experiment. Starting with the composition taken from the equilibrium calculated at a fixed mixture fraction as described above, we increase the OH fraction above its equilibrium value, while also increasing the fractions of H and O atoms in proportions consistent with those derived from the assumption of partial equilibrium. Subsequently, the temperature of the resultant "nonequilibrium" composition is varied until the enthalpy of this composition is equal to that of the initial "equilibrium" composition. At the mixture fraction at the peak of the OH profile, we observe that increasing the OH fraction by a factor of 2 results in a change in temperature of less than 10 K. Therefore, any radical nonequilibrium has no significant relevance for the ∼200 K temperature difference observed between the measurement/computations and equilibrium.

We attribute the observed difference between the equilibrium temperature at a given mixture fraction which was derived as mentioned above by assuming perfectly mixed streams and that calculated in the "full-chemistry" simulations to differential diffusion. While the importance of differential diffusion of molecular hydrogen in turbulent diffusion[27] and MILD flames[28] has been emphasized, predominantly from the perspective of 1-D simulations, differential diffusion is clearly present in the axisymmetric 2-D system studied here. As is well known, the local elemental composition of a chemically reacting gas flow is completely determined by the mixture fraction only if the diffusion coefficients of all components are the same.[29] In that case, the local enthalpy is also directly related to the mixture fraction. In general, the diffusion coefficients of flame species are different, and the local elemental composition cannot be presented as that of a perfect mixture of $\xi$ kg fuel and $(1 - \xi)$ kg oxidizer. More importantly, for estimating the flame temperature, differential diffusion breaks the direct relation between the mixture fraction and the local enthalpy. The presence of differential diffusion is illustrated by Figure 7b, where the mixture fractions along the flame axis are calculated separately for the carbon and hydrogen element fractions obtained from the species mole fractions from the "full-chemistry" solution. As can be seen, the mixture fractions derived from carbon and hydrogen elements do not collapse into one curve but are shifted relative to each other; the axial position for the stoichiometric mixture fractions is shifted by ∼2 mm and by significantly more at other $\xi$. Therefore, differential diffusion in this system makes it impossible to deduce the distribution of the elements' fractions


https://doi.org/10.1021/acs.energyfuels.1c00583
Energy Fuels 2021, 35, 6798−6806

along the centerline based only on the input streams. Consequently, while one can certainly assign a mixture fraction based on the input streams to every point in the flow, the relationship between this mixture fraction and other (thermodynamic) quantities is problematical.

The impact of differential diffusion on the calculated equilibrium temperature is verified by performing equilibrium calculations without using the mixture fraction to derive the input parameters in the thermodynamic calculations. Results of these calculations, where the local elemental composition and enthalpy are taken from "full-chemistry" numerical simulations, are also shown in Figure 7a. As can be seen, the difference between the axial temperatures based on "full-chemistry" and the "equilibrium based on local composition" just described is less than 25 K. This observation also confirms the previous statement that nonequilibrium concentrations of radicals have only a marginal impact on the flame temperature. Furthermore, using the detailed composition rather than the mixture fraction provides a meaningful method for analyzing the degree of nonequilibrium for a given species. As an illustration, the equilibrium OH fraction corresponding to the measured/"full-chemistry" temperature profile in Figure 7a is shown in Figure 7c. Comparison of the equilibrium OH profile computed from the local conditions with the "full-chemistry" profile shows superequilibrium OH fractions roughly three times higher than equilibrium, similar to that reported for other methane/air diffusion flames.[7]

## 4. CONCLUSIONS

Measurements of the distribution of OH radical mole fractions under conditions of MILD combustion in an LJHC burner are presented and discussed using numerical computations of the flame structure presented previously.[6] The OH mole fractions are obtained from LIF measurements and are quantified using direct laser absorption in premixed flames on a flat-flame burner, corrected for local temperature and quenching from spontaneous Raman measurements in the MILD flame, and supported using numerical computations of the 1-D OH fraction. The OH distribution as a whole appears in the wishbone form similar to that in laminar diffusion flames.[8] Allowing for small axial shifts between computations and measurement and for the spatial resolution of the OH measurements, the radial OH profiles are in good agreement with the numerical computations. The maximum OH fractions, roughly 700 ppm, are seen to be more than five times lower than those measured in diffusion flames of methane.[7,8] The axial OH profile shows that the OH fraction peaks on the lean side of the stoichiometric mixture fraction, as do the radial profiles, also typical for the diffusion flame structure. Comparison of the maximum axial OH fractions shows that the numerical results slightly overpredict the experimental result. Analysis of the numerical results shows that the OH mole fraction is in partial equilibrium for mixture fractions that are stoichiometric or leaner, suggesting the use of partial equilibrium in describing MILD combustion under turbulent conditions.

Comparison of the OH fractions with full thermodynamic equilibrium, based on the compositions and enthalpies of the fuel and oxidizer streams, is frustrated by the observation that the maximum measured and computed axial temperature is ~200 K below the equilibrium stoichiometric value. Varying the OH fraction in equilibrium calculations demonstrates that possible superequilibrium OH fractions have essentially no effect on the difference in temperature with thermodynamic equilibrium. Computation of the equilibrium temperature using the elemental composition and enthalpy from the detailed computation shows that the temperatures at stoichiometric or leaner mixture fractions are within 25 K of those at equilibrium. Computing the equilibrium OH fraction using the elemental composition and temperature from detailed computation shows that the measurement/detailed computation is roughly a factor of 3 above equilibrium. The changes in element balance caused by differential diffusion render the use of the mixture fraction to derive local temperature and species fractions problematical in these systems.

## AUTHOR INFORMATION


### Corresponding Author

**A. V. Mokhov** − *Energy Conversion, Energy and Sustainability Research Institute, University of Groningen, Groningen 9747 AG, The Netherlands;* orcid.org/0000-0002-5791-7528; Email: a.v.mokhov@rug.nl

### Authors

**S. B. Nourani Najafi** − *Energy Conversion, Energy and Sustainability Research Institute, University of Groningen, Groningen 9747 AG, The Netherlands*

**J. A. van Oijen** − *Power and Flow, Mechanical Engineering, Eindhoven University of Technology, Eindhoven 5600 MB, The Netherlands*

**H. B. Levinsky** − *Energy Conversion, Energy and Sustainability Research Institute, University of Groningen, Groningen 9747 AG, The Netherlands*

Complete contact information is available at: https://pubs.acs.org/10.1021/acs.energyfuels.1c00583


### Notes

The authors declare no competing financial interest.

## ACKNOWLEDGMENTS

The authors would like to express their thanks to L. Dai, M. van Meurs, D. J. Heusinkveld, and M. Nieuwenhuis, University of Groningen, The Netherlands.

## ABBREVIATIONS

1-D = one-dimensional
2-D = two-dimensional
$\xi$ = mixture fraction
$\xi^{st}$ = stoichiometric mixture fraction
LIF = laser-induced fluorescence
PLIF = planar laser-induced fluorescence
MILD = moderate or intense low-oxygen-dilution
JHC = jet in hot coflow
LJHC = laminar-jet-in-hot-co-flow
$Q$ = collisional deactivation rate
$Z$ = partition function
$S_{line}$ = spectral line strength
$C$ = the proportionality constant
$\varphi$ = equivalence ratio
$z$ = axial distance from fuel tube exit
$r$ = radial distance
ppm = parts per million
$K$ = equilibrium constant


https://doi.org/10.1021/acs.energyfuels.1c00583
Energy Fuels 2021, 35, 6798−6806

## REFERENCES


(1) Cavaliere, A.; de Joannon, M. Mild combustion. *Prog. Energy Combust. Sci.* **2004**, *30*, 329−366.
(2) Dally, B. B.; Karpetis, A. N.; Barlow, R. S. Structure of turbulent non-premixed jet flames in a diluted hot coflow. *Proc. Combust. Inst.* **2002**, *29*, 1147−1154.
(3) Salavati-Zadeh, A.; Esfahanian, V.; Nourani Najafi, S. B.; Saeed, H.; Mohammadi, M. Kinetic simulation of flameless burners with methane/hydrogen blended fuel: Effects of molecular diffusion and Schmidt number. *Int. J. Hydrogen Energy* **2018**, *43*, 5972−5983.
(4) Ye, J.; Medwell, P. R.; Dally, B. B.; Evans, M. J. The transition of ethanol flames from conventional to MILD combustion. *Combust. Flame* **2016**, *171*, 173−184.
(5) Medwell, P. R.; Kalt, P. A. M.; Dally, B. B. Simultaneous imaging of OH, formaldehyde, and temperature of turbulent non-premixed jet flames in a heated and diluted coflow. *Combust. Flame* **2007**, *148*, 48−61.
(6) Abtahizadeh, E.; Sepman, A.; Hernández-Pérez, F.; Van Oijen, J.; Mokhov, A.; De Goey, P.; Levinsky, H. Numerical and experimental investigations on the influence of preheating and dilution on transition of laminar coflow diffusion flames to Mild combustion regime. *Combust. Flame* **2013**, *160*, 2359−2374.
(7) Smyth, K. C.; Tjossem, P. J. H.; Hamins, A.; Miller, J. H. Concentration measurements of OH and equilibrium analysis in a laminar Methane-Air diffusion flame. *Combust. Flame* **1990**, *79*, 366−380.
(8) Smooke, M. D.; Xu, Y.; Zurn, R. M.; Lin, P.; Frank, J. H.; Long, M. B. Computational and experimental study of OH and CH radicals in axisymmetric laminar diffusion flames. *Symp. Combust.* **1992**, *24*, 813−821.
(9) Choi, B. C.; Chung, S. H. Autoignited laminar lifted flames of methane/hydrogen mixtures in heated coflow air. *Combust. Flame* **2012**, *159*, 1481−1488.
(10) Sepman, A. V.; Mokhov, A. V.; Levinsky, H. B. Spatial structure and NO formation of a laminar methane-nitrogen jet in hot coflow under MILD conditions: A spontaneous Raman and LIF study. *Fuel* **2013**, *103*, 705−710.
(11) Sepman, A. V.; Abtahizadeh, S. E.; Mokhov, A. V.; Van Oijen, J. A.; Levinsky, H. B.; De Goey, L. P. H. Numerical and experimental studies of the NO formation in laminar coflow diffusion flames on their transition to MILD combustion regime. *Combust. Flame* **2013**, *160*, 1364−1372.
(12) Sepman, A.; Abtahizadeh, E.; Mokhov, A.; Van Oijen, J.; Levinsky, H.; De Goey, P. Experimental and numerical studies of the effects of hydrogen addition on the structure of a laminar methane-nitrogen jet in hot coflow under MILD conditions. *Int. J. Hydrogen Energy* **2013**, *38*, 13802−13811.
(13) Westbrook, C. K.; Dryer, F. L. Chemical kinetic modeling of hydrocarbon combustion. *Prog. Energy Combust. Sci.* **1984**, *10*, 1−57.
(14) Curran, H. J. Developing detailed chemical kinetic mechanisms for fuel combustion. *Proc. Combust. Inst.* **2019**, *37*, 57−81.
(15) Arndt, C. M.; Schießl, R.; Gounder, J. D.; Meier, W.; Aigner, M. Flame stabilization and auto-ignition of pulsed methane jets in a hot coflow: Influence of temperature. *Proc. Combust. Inst.* **2013**, *34*, 1483−1490.
(16) Evans, M. J.; Medwell, P. R.; Tian, Z. F.; Ye, J.; Frassoldati, A.; Cuoci, A. Effects of oxidant stream composition on non-premixed laminar flames with heated and diluted coflows. *Combust. Flame* **2017**, *178*, 297−310.
(17) Sepman, A. V.; Toro, V. V.; Mokhov, A. V.; Levinsky, H. B. Determination of temperature and concentrations of main components in flames by fitting measured Raman spectra. *J. Appl. Phys. B* **2013**, *112*, 35−47.
(18) Eckbreth, A. C. *Laser Diagnostics for Combustion Temperature and Species*; Gordon and Breach Publishers, 1996; p 391.
(19) Luque, J.; Crosley, D. R. *LIFBASE: Database and Spectral Simulation Program*, version 1.5, SRI International Report MP 99-009, 1999.
(20) Tamura, M.; Berg, P. A.; Harrington, J. E.; Luque, J.; Jeffries, J. B.; Smith, G. P.; Crosley, D. R. Collisional Quenching of CH(A), OH(A), and NO(A) in Low Pressure Hydrocarbon Flames. *Combust. Flame* **1998**, *114*, 502−514.
(21) Kee, R.; Grcar, J.; Smooke, M.; Miller, J.; Meeks, E. PREMIX: a fortran program for modeling steady laminar one-dimensional premixed flames. *Sandia Report*; Sandia National Laboratories; 1985; Vol. *143*.
(22) Smith, G. P.; Golden, D. M.; Frenklach, M.; Moriarty, N. W.; Eiteneer, B.; Goldenberg, M. *GRI-Mech 3.0*, 2000, http://combustion.berkeley.edu/gri-mech/.
(23) Bilger, R. W.; Stårner, S. H.; Kee, R. J. On reduced mechanisms for methane air combustion in non-premixed flames. *Combust. Flame* **1990**, *80*, 135−149.
(24) Lewis, B.; Elbe, G. V. *Combustion, Flames and Explosions of Gases*; Harcourt Brace Jovanovich: Pennsylvania, 1987; pp 231−232.
(25) Medwell, P. R.; Kalt, P. A. M.; Dally, B. B. Imaging of diluted turbulent ethylene flames stabilized on a Jet in Hot Coflow (JHC) burner. *Combust. Flame* **2008**, *152*, 100−113.
(26) Warnatz, J. Concentration, Pressure, and Temperature Dependence of the Flame Velocity in Hydrogen-Oxygen-Nitrogen Mixtures. *Combust. Sci. Technol.* **1981**, *26*, 203−213.
(27) Sutherland, J. C.; Smith, P. J.; Chen, J. H. Quantification of differential diffusion in nonpremixed systems. *Combust. Theory Modell.* **2005**, *9*, 365−383.
(28) Abtahizadeh, E.; De Goey, P.; Van Oijen, J. LES of Delft Jet-in-Hot Coflow burner to investigate the effect of preferential diffusion on autoignition of CH4/H2 flames. *Fuel* **2017**, *191*, 36−45.
(29) Libby, P. A.; Williams, F. A. *Turbulent Reacting Flows*; Springer, 1980; pp 69−71.



https://doi.org/10.1021/acs.energyfuels.1c00583
*Energy Fuels* 2021, 35, 6798−6806